

Quench dynamics across quantum critical points

K. Sengupta, Stephen Powell, and Subir Sachdev

Department of Physics, Yale University, P.O. Box 208120, New Haven, Connecticut 06520-8120, USA

(Received 25 November 2003; published 18 May 2004)

We study the quantum dynamics of a number of model systems as their coupling constants are changed rapidly across a quantum critical point. The primary motivation is provided by the recent experiments of Greiner *et al.* [Nature (London) **415**, 39 (2002)] who studied the response of a Mott insulator of ultracold atoms in an optical lattice to a strong potential gradient. In a previous work, it had been argued that the resonant response observed at a critical potential gradient could be understood by proximity to an Ising quantum critical point describing the onset of density wave order. Here we obtain numerical results on the evolution of the density wave order as the potential gradient is scanned across the quantum critical point. This is supplemented by studies of the integrable quantum Ising spin chain in a transverse field, where we obtain exact results for the evolution of the Ising order correlations under a time-dependent transverse field. We also study the evolution of transverse superfluid order in the three-dimensional case. In all cases, the order parameter is best enhanced in the vicinity of the quantum critical point.

DOI: 10.1103/PhysRevA.69.053616

PACS number(s): 03.75.Kk, 05.30.-d

I. INTRODUCTION

Recent experiments with ultracold atoms have achieved reversible tuning of bosonic atoms between superfluid and Mott insulating states by varying the strength of periodic potential produced by standing laser light [1,2]. The physics of such ultracold atoms in the Mott insulating state can be described by bosonic Hubbard model, well known in context of other condensed-matter systems [3,4]. However, ultracold atoms in optical lattices offer much better control over microscopic parameters of the model. Consequently, it is possible to explore parameter regimes which are not available in other analogous condensed-matter systems.

This paper will focus on a particular experiment reported by Greiner *et al.* [1]. With the boson system in the Mott insulating state, they applied a steep potential gradient to the lattice, and observed its response. In a typical condensed-matter system, one might have expected a response analogous to that of a sliding charge-density wave: no motion of atoms until a critical tilt was applied, and a sliding motion at all tilts above the critical tilt. However, the experiment observed strikingly different behavior: there was a strong *resonant* response in the vicinity of tilts where the potential-energy drop between nearest-neighbor optical lattice sites (E) equaled the repulsion between two atoms on the same site (U). For $E \sim U$, applying the tilt produced a noticeable change in the ground state, but (in contrast to sliding charge-density wave systems) there was little change in the ground state for larger E until a second resonant peak at $E \sim 2U$. This resonant response is a clear indication that the atoms experience little extrinsic dissipation, and their dynamics should be described by an energy-conserving quantum Hamiltonian.

A framework for describing the experiments of Greiner *et al.* [1] was proposed in Ref. [5] (hereafter referred to as I). (We also note here the numerical studies of Braun-Munzinger *et al.* [6] which addressed these experiments by studying the time evolution of the underlying Bose-Hubbard

model.) For w , $|E-U| \ll E, U$, where w is the tunneling matrix element between nearest-neighbor lattice sites, it was argued that we need only focus on a set of states which were *resonantly coupled* to the original Mott insulating state. In one dimension, the resonant subspace could be described simply in terms of nearest-neighbor *dipole* states, consisting of a particle and a hole excitation about the Mott insulator on nearest-neighbor sites; in higher dimensions, the particle and hole were no longer constrained to be on nearest-neighbor sites but could reside anywhere on planes orthogonal to the potential gradient, but separated by a single lattice spacing. An effective Hamiltonian on such resonant subspaces was proposed in I, and its phase diagram was presented. In the regime of large potential gradient $E-U > w$, this effective Hamiltonian possessed ground states with density wave order with a period of two lattice spacings (see also Ref. [8] for conditions under which other periods may obtain). It was argued in I that the proximity of the quantum critical point, associated with the onset of this density wave order, was responsible for the resonant response observed by Greiner *et al.*

The tilt experiments of Greiner *et al.* were carried out in highly nonequilibrium situations, and the approach of I was to describe these, to the extent possible, by an equilibrium analysis of an effective Hamiltonian describing the primary states accessed over the experimental time scale. The purpose of the present paper is to directly address the nonequilibrium dynamics of the tilted Mott insulator. We will mainly do this using the effective Hamiltonian of I. The specific question we shall address is the following. Begin with the system in the ground state in a regime of small $E=E_i$ where there is no density wave order. Then, suddenly change the value of E to a $E=E_f$, including values such that the ground state has density wave order at E_f . Allow the system to evolve under the resulting Hamiltonian. What is the nature of the state to which the system evolves at long times? We will find, as conjectured in I, that the density wave order that develops under this dynamic evolution is most robust when E_f is near the quantum critical point.

We will also address a similar question for the Ising chain in a transverse field, g . Like the models of I, this model also has a regime $g < g_c$ where the ground state has spontaneous Ising order. However, this much simpler model is completely integrable, and so offers an opportunity to analyze the non-equilibrium dynamics exactly. We initialize the Ising model in the ground state in a transverse field $g_i > g_c$. The transverse field is then changed rapidly to $g = g_f$, and the wave function evolves at this field. We will compute equal-time correlations in this wave function as a function of the time t , including in the $t \rightarrow \infty$ limit. In some cases, exact closed-form results will be obtained. The structure of these correlations as a function of g_f bears some similarity to the results of the model of I as a function of E_f ; however, there are some interesting differences which, we suspect, are related to the integrability of the Ising chain.

We now outline the remainder of the paper. In Sec. II we present numerical results on the dynamics of the one-dimensional dipole model of I. Section III will address the nonequilibrium dynamics of the Ising chain in a transverse field: this analysis uses the Jordan-Wigner transformation, and obtains the required dynamic correlation functions in the form of Toeplitz determinants. Section IV returns to the model of I, but turns to the dynamics in three dimensions; here, we use a combination of mean-field theory and exact diagonalization to obtain results similar to those in Sec. II, but with the order parameter now being a ‘‘transverse superfluid’’ order. We review the results and discuss implications for experiments in Sec. V.

II. DIPOLE DYNAMICS IN ONE DIMENSION

This section will describe our numerical results on the quantum dynamics of the one-dimensional (1D) dipole model of the Mott insulator in a potential gradient.

Starting from a parent Mott state with n_0 bosons per site, we identified the set of states which are resonantly coupled to the parent Mott state when $U \sim E$ (recall that U is the repulsive energy between two bosons on the same site, and E , the ‘‘electric field,’’ is the potential drop between two nearest-neighbor sites). In one dimension, the resonant subspace involves dipole states consisting of quasihole-quasiparticle pairs at adjacent sites, and the low-energy behavior of the system can be described by the effective dipole Hamiltonian obtained in I:

$$H_{1D}[E] = -w\sqrt{n_0(n_0+1)}\sum_{\ell}(d_{\ell}^{\dagger}+d_{\ell})+(U-E)\sum_{\ell}d_{\ell}^{\dagger}d_{\ell}. \quad (1)$$

The dipoles are subject to hard-core constraints that there is never more than a single dipole on any pair of nearest-neighbor sites,

$$d_{\ell}^{\dagger}d_{\ell} \leq 1, \quad d_{\ell+1}^{\dagger}d_{\ell+1}d_{\ell}^{\dagger}d_{\ell} = 0. \quad (2)$$

When the electric field E is adiabatically tuned through U , the ground state of the system changes from one with no dipoles ($U \gg E$) to one with maximum possible number of dipoles ($E \gg U$). At an intermediate critical electric field

$$E_c = U + 1.310w\sqrt{n_0(n_0+1)}, \quad (3)$$

the system undergoes a quantum phase transition in the Ising universality class.

As discussed in Sec. I, we study the dynamics of the ultracold atoms when the potential gradient is changed suddenly. Such a situation can be very easily achieved experimentally in these systems by rapidly shifting the center of the confining magnetic trap. We shall specifically consider the situation where the change in the potential gradient is fast enough for the sudden perturbation assumption to be valid but slow enough to restrict the dynamics within the resonant subspaces so that the Hamiltonian (1) [and Eq. (26) in Sec. IV] is still valid.

We assume that the atoms in the 1D lattice are initially in the ground state $|\Psi_G\rangle$ of the dipole Hamiltonian (1) with $E = E_i \ll E_c$. This ground state corresponds to dipole vacuum. Consider shifting the center of the magnetic trap so that the new potential gradient is E_f . If this change is done suddenly, the system initially remains in the old ground state. The state of the system at time t is therefore given by

$$|\Psi(t)\rangle = \sum_n c_n \exp(-i\epsilon_n t/\hbar)|n\rangle, \quad (4)$$

where $|n\rangle$ denotes the complete set of energy eigenstates of the Hamiltonian $H_{1D}[E_f]$ in Eq. (1), $\epsilon_n = \langle n|H_{1D}[E_f]|n\rangle$ is the energy eigenvalue corresponding to state $|n\rangle$, and $c_n = \langle n|\Psi(t=0)\rangle = \langle n|\Psi_G\rangle$ denotes the overlap of the old ground state with the state $|n\rangle$. Notice that the state $|\Psi(t)\rangle$ is no longer the ground state of the new Hamiltonian. Furthermore, in the absence of any dissipative mechanism, which is the case for ultracold atoms in optical lattices, $|\Psi(t)\rangle$ will never reach the ground state of the new Hamiltonian. Rather, in general, we expect the system to thermalize at long enough times, so that the correlations are similar to those of $H_{1D}[E_f]$ at some finite temperature.

We are now in a position to study the dynamics of the Ising density wave order parameter

$$O = \frac{1}{N}\langle\Psi|\sum_{\ell}(-1)^{\ell}d_{\ell}^{\dagger}d_{\ell}|\Psi\rangle, \quad (5)$$

where N is the number of sites. The time evolution of O is given by

$$O(t) = \frac{1}{N}\sum_{m,n} c_m c_n \cos[(E_m - E_n)t/\hbar] \langle m|\sum_{\ell}(-1)^{\ell}d_{\ell}^{\dagger}d_{\ell}|n\rangle. \quad (6)$$

Equation (6) is solved numerically using exact diagonalization to obtain the eigenstates and eigenvalues of the Hamiltonian $H_{1D}[E_f]$. Before resorting to numerics, it is however useful to discuss the behavior of $O(t)$ qualitatively. We note that if E_f is close to E_i , the old ground state will have a large overlap with new one, i.e., $c_m \sim \delta_{m1}$. Hence in this case we expect $O(t)$ to have small oscillations about $O(t=0)$. On the other hand, if $E_f \gg E_c$, the two ground states will have very little overlap, and we again expect $O(t)$ to have a small oscillation amplitude. This situation is in stark contrast with the

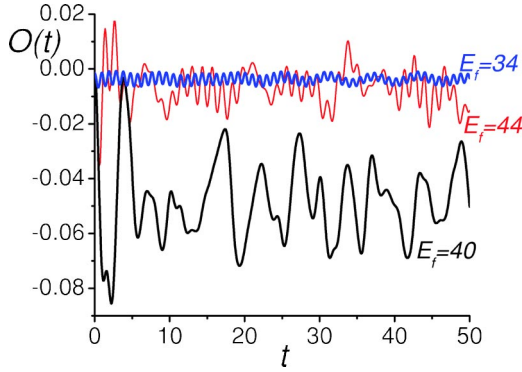


FIG. 1. Evolution of the Ising order parameter in Eq. (5) under the Hamiltonian $H_{1D}[E_f]$ for $n_0=1$. The initial state is the ground state of $H_{1D}[E_i]$. All the plots in this section have $U=40$, $w=1$, and $E_i=32$, and consequently the equilibrium quantum critical point is at $E_c=41.85$.

adiabatic turning on of the potential gradient, where the systems always remain in the ground state of the new Hamiltonian $H_{1D}[E_f]$, and therefore has a maximal value of $\langle O \rangle$ for $E_f \gg E_c$. In between, for $E_f \sim E_c$, the ground state $|\Psi\rangle$ has a finite overlap with many states $|m\rangle$, and hence we expect $O(t)$ to display significant oscillations. Furthermore, if the symmetry between the two Ising ordered states is broken slightly (as is the case in our studies below), the time-average value of $O(t)$ will be nonzero.

This qualitative discussion is supported by numerical calculations on finite-size systems for system size $N=9, 11, 13$. For numerical computations with finite systems, we choose systems with an odd number of sites and open boundary conditions, so that dipole formation on odd sites is favored, thus breaking the Z_2 symmetry. The results are shown in Figs. 1–4. Figure 1 shows the oscillation of the order parameter $O(t)$ for different values of E_f for $N=13$. In agreement with our qualitative expectations, the oscillations have maximum amplitude when $E_f \approx 40$ is near the critical value $E_c = 41.85$. For either $E_f \leq E_c$ or $E_f \gg E_c$, the oscillations have a small amplitude around $O(t=0)$. Furthermore, it is only for $E_f \approx E_c$ that the time-average value of $O(t)$ is appreciable. Figure 2 shows the system size dependence of the time evolution for $E_f=U=40$. We find that the oscillations remain

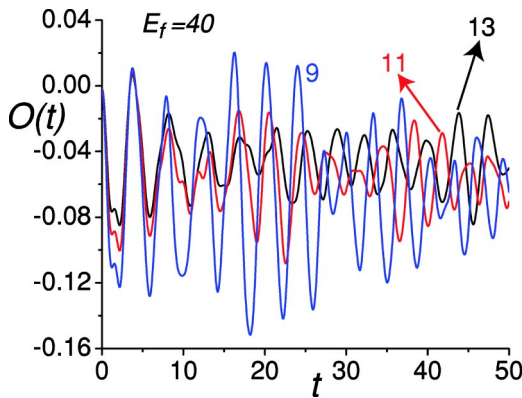


FIG. 2. System size (N) dependence of the results of Fig. 1 for $E_f=40$. The curves are labeled by the value of N .

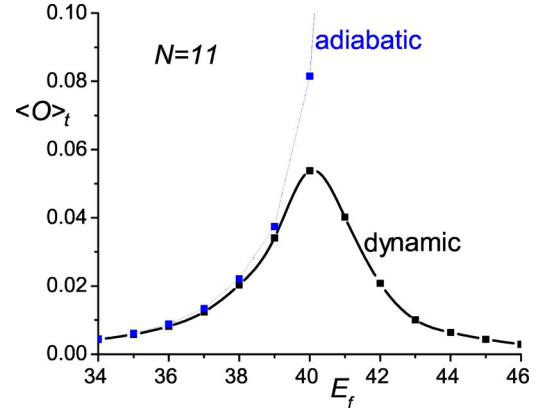


FIG. 3. The curve labeled “dynamic” is the long-time limit $\langle O \rangle_t$ of the Ising order in Eq. (6) as a function of E_f (for $N=11$), with other parameters as in Fig. 1. This long-time limit can be obtained simply by setting $m=n$ in Eq. (6). For comparison, in the curve labeled “adiabatic,” we show the expectation value of the Ising order O in the ground state of $H_{1D}[E_f]$; such an order would be observed if the value of E was changed adiabatically. Note that the dynamic curve has its maximal value near (but not exactly at) the equilibrium quantum critical point $E_c=41.85$, where the system is able to respond most easily to the change in value of E ; this dynamic curve is our theory of the “resonant” response in the experiments of Ref. [1] discussed in Sec. I. In contrast the adiabatic result *increases monotonically* with E_f into the $E > E_c$ phase where the Ising symmetry is spontaneously broken.

visible as we go to higher system sizes, although they do weaken somewhat. More significantly, the time-average value of $O(t)$ remains nonzero, and has a weaker decrease with system size. In Fig. 3, we plot the long-time limit of the Ising order parameter, $\langle O \rangle_t$, as a function of E_f , and compare it with the O_{ad} , the value of the order parameter when E reaches E_f adiabatically and the wave function is that of the ground state at $E=E_f$. We find that $\langle O \rangle_t$ stays close to O_{ad} as long as there is a large overlap between the old and the new ground states. However, as we approach the adiabatic phase

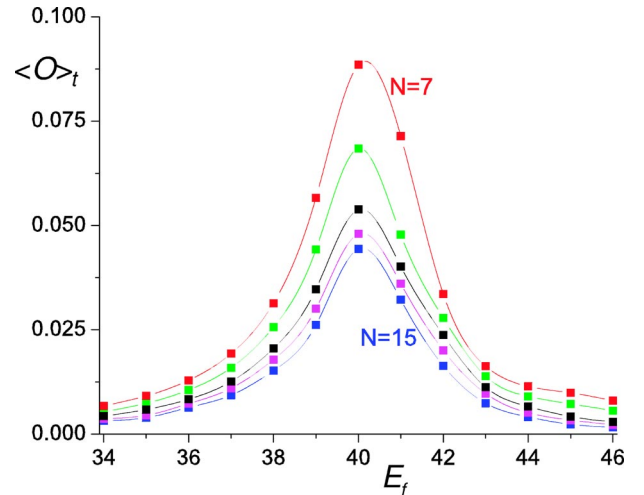


FIG. 4. Size dependence of the “dynamic” results in Fig. 3. The sizes range from $N=7$ to $N=15$ (as labeled), with the intermediate values $N=9, 11, 13$: $\langle O \rangle_t$ decreases monotonically with N .

transition point, this overlap decreases and $\langle O \rangle_t$ cannot follow O_{ad} anymore. The deviation of $\langle O \rangle_t$ is therefore a signature that the system is now in a different phase for the new value of the electric field.

The “dynamic” curve in Fig. 3 should be compared with Figs. 5(e) and 5(f) in Ref. [1]. The latter show that the Mott insulator has a resonantly strong response to an applied potential gradient $E \sim U$. Here, we have found a similar resonant enhancement in a simple model system in one dimension, induced by the proximity of a quantum critical point.

We comment briefly on the nature of the thermodynamic limit $N \rightarrow \infty$ for the results in Figs. 2 and 3. For O_{ad} it is clear that there is a nonzero limit only for $E > E_c$, when it equals the order parameter of the spontaneously broken Ising symmetry. If we assume that the system thermalizes at long times for the dynamic case, then $\langle O \rangle_t$ corresponds to the expectation value of the equilibrium order parameter in $H_{1D}[E_f]$ at some finite temperature. In one dimension, it is not possible to break a discrete symmetry at finite temperatures, and so the thermodynamic limit of the order parameter must always vanish. By this reasoning, we expect $\langle O \rangle_t$ to also vanish in the thermodynamic limit. This is consistent with the results in Fig. 4, where we show the N dependence of the long-time limit $\langle O \rangle_t$. Our data are at present not extensive enough to definitely characterize the dependence of $\langle O \rangle_t$ on N .

III. DYNAMICS OF THE QUANTUM ISING CHAIN

As a complement to the physically relevant, but numerical, computations in Sec. II, this section will describe similar results in a simpler, analytically tractable model. We will consider the integrable Ising chain in a transverse field, which also has a zero-temperature, quantum phase transition between a phase with a broken Z_2 symmetry and a symmetric phase. We will address questions on the evolution of the wave function under a time-dependent change in the transverse field. Different aspects of the nonequilibrium dynamics of the Ising chain were studied earlier by Iglói and Rieger [7] using similar methods.

The model of interest in this section is

$$H_I = -J \sum_j [\sigma_j^z \sigma_{j+1}^z + g(t) \sigma_j^x], \quad (7)$$

where $\sigma_j^{x,z}$ are Pauli matrices acting on a “spin” on the sites j of an infinite chain. We have allowed the transverse field to acquire an arbitrary time dependence $g(t)$. We will mainly consider here the case of a sudden change at time $t=0$ from an initial value $g(0^-) = g_i$ to a final value $g(0^+) = g_f$, but our methods easily generalize to the arbitrary time dependence in $g(t)$.

For time independent $g(t)$, H_I has a quantum critical point at $g = g_c = 1$, with two equivalent ground states for $g < g_c$ related by a global Z_2 spin flip. However, unlike Sec. II we will not introduce any external perturbation which introduces a preference between these two states: all such perturbations destroy the integrability of H_I . Consequently, we do not obtain any useful information from the analog of the time dependence of the order parameter in Eqs. (5) and (6), as these

quantities will be identically zero at all times. Rather, we will compute here the two-point correlation function of the order parameter in an infinite chain, which is

$$G_n(t) = \langle \psi(t) | \sigma_j^z \sigma_{j+n}^z | \psi(t) \rangle. \quad (8)$$

Here $|\psi(t)\rangle$ is the state of the system at time t , evolving under the Schrödinger equation specified by the time-dependent Hamiltonian H_I . In equilibrium, the information contained in a correlation function like Eq. (8) is related to an observable like that in Eq. (6) (which is the response in the Ising order parameter to perturbations in the boundary condition) by the fluctuation-dissipation theorem. However, we are not aware of any analog of such a theorem for the nonequilibrium case under consideration here, and so are not able to directly relate the results of the present section to those of Sec. II.

Our analysis of H_I proceeds with the standard Jordan-Wigner transformation, and we follow the notation and methods of Chap. 4 of Ref. [4]. We express the $S=1/2$ states in terms of those of the spinless Jordan-Wigner fermion c_j , and after transforming to momentum space fermions c_k , the Hamiltonian becomes

$$H_I = J \sum_k [2(g - \cos k) c_k^\dagger c_k - i \sin k (c_{-k}^\dagger c_k^\dagger + c_{-k} c_k) - g]. \quad (9)$$

Now, transforming to the Heisenberg picture, we can follow the evolution of the system by solving the equations of motion

$$\frac{dc_k}{dt} = i[H_I, c_k]. \quad (10)$$

These equations are easily solved by a Bogoliubov transformation. Finally, the correlator in (8) is computed by a simple generalization of the methods appropriate for the equilibrium case. A few details of such a computation appear in the Appendix.

Here, we discuss the results for $G_n(t)$ for the case of a sudden change from $g(0^-) = g_i$ to $g(0^+) = g_f$. For $t < 0$, we assume the system is in the ground state appropriate for $g = g_i$, and consequently $G_n(t < 0)$ is independent of t and equal to the well-known equilibrium result at $g = g_i$. For $t > 0$, there is a nontrivial time dependence, and it is possible to obtain the general expression for $G_n(t)$ as described in the Appendix. We will restrict our attention here to the simpler expression of the long-time limit $G_n(t \rightarrow \infty)$, which is the primary quantity of physical interest. For this, we obtain the Toeplitz determinant

$$G_n(\infty) = \begin{vmatrix} a_0 & a_{-1} & \cdots & a_{-n+1} \\ a_1 & a_0 & \cdots & a_{-n+2} \\ \vdots & \vdots & \ddots & \vdots \\ a_{n-1} & a_{n-2} & \cdots & a_0 \end{vmatrix}, \quad (11)$$

where

$$a_r = \frac{1}{2\pi} \int_{-\pi}^{\pi} e^{-ikr} \tilde{a}(k), \quad (12)$$

with

$$\tilde{a}(k) = \frac{2(g_f g_i + 1)z - (g_f + g_i)(z^2 + 1)}{2(z - g_f)} \sqrt{\frac{z}{(z - g_i)(1 - z g_i)}}, \quad (13)$$

where $z = e^{ik}$.

We now need to evaluate the $n \times n$ Toeplitz determinant in Eq. (11), especially for the case of large n . In the equilibrium situation, this is aided by Szegő's lemma, and its generalization in the Fisher-Hartwig formula [9]. For the present situation, the expression in Eq. (13) does not obey the winding number constraint required for application of the Fisher-Hartwig formula, and so we are unable to take advantage of this result. However, we shall show that an exact evaluation of Eq. (11) is possible for two important special cases ($g_i = \infty$ and $g_i = 0$), and supplement these by numerical evaluation of Eq. (11) for other values of g_i .

In the case $g_i = 0$, we have

$$\tilde{a}(k) = \frac{2z - g_f(z^2 + 1)}{2(z - g_f)} \quad (14)$$

and it is straightforward to evaluate a_r by contour integration. This gives

	$g_f < 1$	$g_f > 1$
$r \leq -1$	$\frac{g_f^{-r}}{2}(1 - g_f^2)$	0
$r = 0$	$1 - \frac{g_f^2}{2}$	$\frac{1}{2}$
$r = 1$	$-\frac{g_f}{2}$	$-\frac{1}{2g_f}$
$r \geq 2$	0	$\frac{g_f^{-r}}{2}(g_f^2 - 1)$

(15)

For the case $g_i = +\infty$, we have

$$\tilde{a}(k) = \frac{2g_f z - (z^2 + 1)}{2(z - g_f)} \quad (16)$$

and a_r is given by

	$g_f < 1$	$g_f > 1$
$r \leq -1$	$-\frac{g_f^{-r-1}}{2}(1 - g_f^2)$	0
$r = 0$	$\frac{g_f}{2}$	$\frac{1}{2g_f}$
$r = 1$	$-\frac{1}{2}$	$\frac{1}{2g_f^2} - 1$
$r \geq 2$	0	$-\frac{1}{2g_f^{r+1}}(g_f^2 - 1)$

(17)

In both of these two cases, the following conditions are met.

Condition 1. For $g_f > 1$, $a_r = 0$ for $r \leq -1$.

Condition 2. For $g_f < 1$, $a_r = 0$ for $r \geq 2$.

Condition 3. For $g_f < 1$, $a_r = g_f a_{r+1}$ for $r \leq -2$.

Using condition 1, we can immediately write $G_n(\infty) = a_0^n$ for $g_f > 1$. For $g_f < 1$, define

$$D_n^r = \begin{vmatrix} a_{-r} & a_{-r-1} & \cdots & a_{-r-n+1} \\ a_1 & a_0 & \cdots & a_{-n+2} \\ \vdots & \vdots & \ddots & \vdots \\ a_{n-1} & a_{n-2} & \cdots & a_0 \end{vmatrix}, \quad (18)$$

so that $G_n(\infty) = D_n^0$. Condition 2 gives $D_n^r = a_{-r} D_{n-1}^0 - a_1 D_{n-1}^{r+1}$ and condition 3 gives $D_n^r = g_f D_n^{r-1}$ for $r \geq 2$. Also, $D_1^r = a_{-r}$. We can therefore write

$$\begin{pmatrix} D_n^0 \\ D_n^1 \end{pmatrix} = \begin{pmatrix} a_0 & -a_1 \\ a_{-1} & -a_1 g_f \end{pmatrix} \begin{pmatrix} D_{n-1}^0 \\ D_{n-1}^1 \end{pmatrix} \quad (19)$$

$$= \begin{pmatrix} a_0 & -a_1 \\ a_{-1} & -a_1 g_f \end{pmatrix}^{n-1} \begin{pmatrix} D_1^0 \\ D_1^1 \end{pmatrix} \quad (20)$$

$$= \begin{pmatrix} a_0 & -a_1 \\ a_{-1} & -a_1 g_f \end{pmatrix}^n \begin{pmatrix} 1 \\ 0 \end{pmatrix}. \quad (21)$$

This can be evaluated by diagonalizing the matrix.

Collecting all the analytic results above, we have for the case $g_i = 0$

$$G_n(\infty) = \begin{cases} \frac{g_f^{n+1}}{2^n} \cosh \left[(n+1) \ln \left(\frac{1 + \sqrt{1 - g_f^2}}{g_f} \right) \right] & \text{for } g_f \leq 1 \\ \left(\frac{1}{2} \right)^n & \text{for } g_f \geq 1. \end{cases} \quad (22)$$

In the limit that $n \rightarrow \infty$, the result for $g_f < 1$ becomes

$$G_n(\infty) \rightarrow \left(\frac{1 + \sqrt{1 - g_f^2}}{2} \right)^{n+1}. \quad (23)$$

In the case $g_i = +\infty$, the corresponding results are

$$G_n(\infty) = \begin{cases} \left(\frac{1}{2}\right)^n \cos[n \arccos(g_f)] & \text{for } g_f \leq 1 \\ \left(\frac{1}{2g_f}\right)^n & \text{for } g_f \geq 1. \end{cases} \quad (24)$$

Note that there are spatial oscillations in the correlator for the case where the field is reduced from a large positive value ($g_i = +\infty$) to a value below the critical point ($g_f < 1$).

Of these exact results, the case $g_i = \infty$ is the one that corresponds most closely to the physical situation discussed in Sec. II. Here we start from a fully “disordered” initial state, and then suddenly change parameters to values with increasing order (this is the analog of increasing E in Sec. II). For final parameter values $g_f > g_c = 1$, we find here a result quite similar to that found in Sec. II: from Eq. (24) we see that the order-parameter correlations decay with the correlation length ξ_f given by

$$\xi_f = \frac{1}{\ln(2g_f)}. \quad (25)$$

This increases monotonically with decreasing g_f , and is thus similar to the increase in the value of $\langle O \rangle_t$ with increasing E_f for $E_f < E_c$ in Fig. 3. By the analogy with Fig. 3, we would expect here that there is a maximum in ξ_f at $g_f = g_c$. However, we find a somewhat different behavior for $g_f < g_c$ in Eq. (24): the correlations do not decay in a simple exponential, but now oscillate, with the period of oscillation becoming smaller with decreasing g_f . So the correlations of the Ising ordered state are indeed best formed at $g_f = g_c$, but we find an unusual oscillatory decay of correlations for $g_f < g_c$. The oscillations are a clear indication of the absence of thermalization in the present model, and we expect they are special consequence of its integrability.

We extended these analytic results by numerical evaluation of Eq. (11) for other values of g_i , and found closely related behavior. Our results for $g_i = 2$ are shown in Fig. 5, and these are the analog here of the results in Figs. 3 and 4. As g_f is decreased, the correlations become longer ranged, until they reach a maximum range at $g_f = g_c = 1$. At smaller values of g_f , the correlations acquire an oscillatory behavior, but are also clearly shorter ranged. So the Ising order is best developed for g_f near the quantum critical point.

IV. DYNAMICS IN THREE DIMENSIONS

We now return to the “tilted” Mott insulator problem addressed in Sec. II and in I. Here we will address questions of quench dynamics for the three-dimensional case. As discussed at length in I, the resonant subspace in 3D is described by quasiparticles and quasiholes which are free to move in the directions transverse to the applied electric field. Consequently, the dipoles of Sec. II, which are bound quasihole-quasiparticle pairs in adjacent sites, constitute only a small part of the resonant subspace, and an effective Hamiltonian for unbound quasiparticle and quasihole states is necessary. A mean-field theory of this effective Hamiltonian was examined in I, and a fairly complex phase dia-

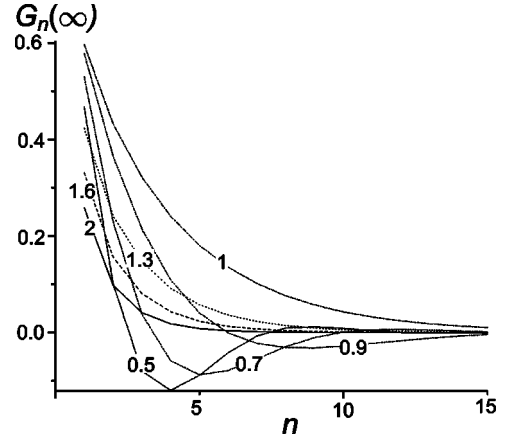


FIG. 5. Ising order correlations defined in Eq. (8). The system is in the ground state of H_I for $t < 0$ with $g = g_i = 2$. At $t = 0^+$, the value of g is changed suddenly to $g = g_f$, and remains at this value for all $t > 0$. Note that at long times, the order is best developed for $g_f = 1$, which is the location of the equilibrium quantum critical point. This result is the analog of Figs. 3 and 4 for the dipole model of Sec. II.

gram was found. In addition to the Ising density wave order that appeared in one dimension, states with a *transverse superfluid* order were present. The latter states correspond to delocalization of the quasiholes and quasiparticles in the direction transverse to the applied electric field.

In this section, we will address the quench dynamics across the transition associated with the onset of transverse superfluid order. This was found to be a second-order transition in the mean-field theory of I, and here we will extend the mean-field theory to an analysis of the nonequilibrium dynamics across the superfluid-insulator transition. We will not examine here the onset of Ising order, already studied in Sec. II; the present mean-field theory found a strong first-order transition for the onset of Ising order. Our analysis will be restricted to the regime where both the superfluid and insulating states have no Ising density wave order.

The effective mean-field Hamiltonian describing the dynamics of these quasiparticles and quasiholes can be written as in I:

$$\begin{aligned} H_{3D}[\langle p_\ell \rangle, \langle h_\ell \rangle; E] &= \sum_\ell \left[-wZ[n_0 h_\ell \langle h_\ell \rangle^* + (n_0 + 1)p_\ell \langle p_\ell \rangle^* + \text{H.c.}] \right. \\ &\quad - w\sqrt{n_0(n_0 + 1)}(p_\ell h_{\ell-1} + \text{H.c.}) + \frac{(U - E)}{2}(p_\ell^\dagger p_\ell + h_\ell^\dagger h_\ell) \\ &\quad \left. - \mu_\ell(p_{\ell+1}^\dagger p_{\ell+1} - h_\ell^\dagger h_\ell) \right]. \end{aligned} \quad (26)$$

Here ℓ is a one-dimensional site index labeling sites along the longitudinal direction of the applied potential gradient (the transverse degrees of freedom are treated in a mean-field approximation and so there is no dependence on the transverse site label), p and h are quasiparticle and quasihole annihilation operators, Z is the number of nearest neighbors

in the transverse directions, and μ_ℓ denotes chemical potential which enforces the constraints

$$\langle p_{\ell+1}^\dagger p_{\ell+1} \rangle = \langle h_\ell^\dagger h_\ell \rangle. \quad (27)$$

Although the Hamiltonian (26) has no nonlinear terms, its diagonalization is nontrivial because of the hard-core constraint on all sites,

$$p_\ell^\dagger p_\ell \leq 1, \quad h_\ell^\dagger h_\ell \leq 1, \quad p_\ell^\dagger p_\ell h_\ell^\dagger h_\ell = 0. \quad (28)$$

The mean fields $\langle p_\ell \rangle$ and $\langle h_\ell \rangle$ correspond to transverse particle/hole superfluid order and were self-consistently determined by diagonalizing the 3D Hamiltonian (26) while maintaining Eq. (28).

We now consider the evolution of the ground state under a sudden shift in the value of E from $E=E_i$ to $E=E_f$ at $t=0^+$. We place E_i in a regime where the ground state preserves all symmetry, and there is neither Ising nor transverse superfluid order. The initial ground state $|\Psi^{3D}\rangle$ will evolve according to the new Hamiltonian $H_{3D}[\langle p \rangle, \langle h \rangle; E_f]$. However, in contrast to the 1D case, here the evolutions of the mean fields $\langle p \rangle$ and $\langle h \rangle$ have to be self-consistently determined. Within time-dependent Hartree approximation, we obtain

$$\begin{aligned} |\Psi^{3D}(t)\rangle &= \sum_m c_m(t) |m\rangle, \\ i\hbar \frac{dc_m(t)}{dt} &= \sum_n c_n(t) \langle n | H_{3D}[\langle p_\ell(t) \rangle, \langle h_\ell(t) \rangle; E_f] | m \rangle, \\ \langle p_\ell(t) \rangle &= \sum_{m,n} c_m^*(t) c_n(t) \langle m | p | n \rangle, \\ \langle h_\ell(t) \rangle &= \sum_{m,n} c_m^*(t) c_n(t) \langle m | h | n \rangle. \end{aligned} \quad (29)$$

We used a basis of states $|n\rangle$ (the final results are, of course, independent of the choice of this basis) which are the complete set of eigenkets of the Hamiltonian $H_{3D}[\langle p_\ell^f \rangle, \langle h_\ell^f \rangle; E_f]$, where $\langle p_\ell^f \rangle$ and $\langle h_\ell^f \rangle$ are the ground-state values of the particle and hole order condensates for $E=E_f$. All the states $|n\rangle$ maintain Eq. (28) exactly, and so these hard-core constraints are fully respected by our calculation: this is what makes diagonalization of the Hamiltonian time consuming and numerically intensive. We note that these equations also maintain the constraints (27) at all ℓ and t .

We examined the above equations for the transverse superfluid order using the same protocol used in Sec. II for the Ising order. The set of Eqs. (29) were solved self-consistently for longitudinal system size $N=4$. We consider the starting potential gradient E_i to be in the insulator phase with neither superfluid nor Ising order, and ramp up the potential gradient to enter the superfluid phase. The gauge symmetry of the superfluid order parameter is broken by adding a small symmetry breaking term $H_{\text{sym}} = -\sum_\ell \eta [p_\ell + h_\ell + \text{H.c.}]$, where η is an infinitesimal positive constant. In the absence of such a symmetry-breaking term we would have $\langle p_\ell \rangle$ and $\langle h_\ell \rangle$ vanish

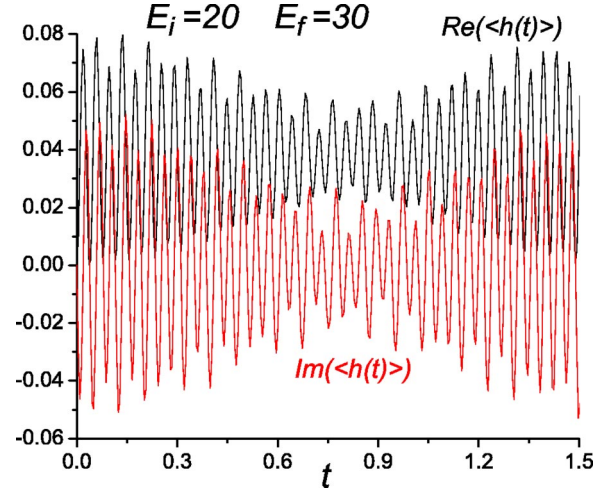


FIG. 6. Oscillations of the hole superfluid order parameter. The plot is shown for $U=40$, $w=1$, $n_0=1$, $Z=4$, $E_i=20$, and $E_f=30$. For these parameters, the quantum critical point is at $E_c=26.4$.

identically for all t by gauge invariance. However, even an infinitesimal symmetry breaking is sufficient, in the suitable parameter regime, to induce appreciable values of the superfluid order. In practice, this symmetry breaking is provided by the coupling of the system to its environment.

With the symmetry-breaking term present, the superfluid order parameters $\langle p_\ell \rangle$ and $\langle h_\ell \rangle$ are initially real. As seen in Fig. 6, $\langle h(t) \rangle = \sum_\ell \langle h_\ell(t) \rangle$ develop coherent oscillations once the potential gradient takes the value E_f . (These results are the analog of Figs. 1 and 2.) The oscillations in $\langle p(t) \rangle$ are similar, but occur with a different period due to the inherent particle-hole asymmetry in Eq. (26). The long-time average of the oscillations is purely real, and this is of course determined by the symmetry-breaking term. Such oscillations of the superfluid order parameter were also obtained recently in a different context in Refs. [10,11] and by Levitov [12].

We also examined the E_f dependence of the long-time average of the superfluid order, and the analog of Fig. 3 appears in Fig. 7. Again the superfluid order is most strongly enhanced in the vicinity of the quantum critical point. However, unlike Fig. 3, we do not observe a precursor to the superfluid order in the insulating phase: this is surely an artifact of the mean-field treatment of the transverse degrees of freedom.

V. CONCLUSIONS

With advent of the study of quantum phase transitions in trapped atomic systems, there is a clear need for theoretical studies in the highly nonequilibrium situations that experiments are often in. In particular, experiments can easily explore the change in the state of the system upon a sudden change in a parameter in the Hamiltonian. There are few general principles in such cases (e.g., there is no fluctuation-dissipation theorem which controls correlations of the final state), and theory is clearly still in its infancy. Two recent studies in this class [10,11] examined the evolution of super-

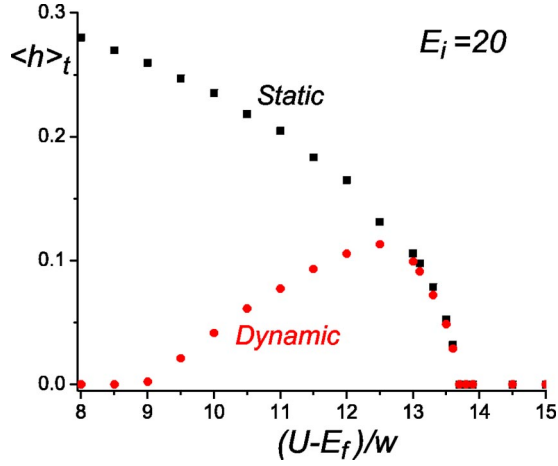


FIG. 7. Analog of Fig. 3, but for the transverse superfluid order, using the same parameters (apart from E_f) as Fig. 3. The “static” curve is the equilibrium superfluid order parameter determined in I. The “dynamic” curve is the long-time average of the real part of $\langle h(t) \rangle$.

fluid order under a sudden change in the optical lattice potential exerted on trapped bosons.

It is clear that exact results on simple solvable models in nonequilibrium situations would be valuable. We have provided such an example here in Sec. III, where we examined the Ising chain in a transverse field, g . This model has a quantum critical point at $g = g_c$, with spontaneous ferromagnetic order in the ground state for $g < g_c$. We started the Ising model in the paramagnetic state ($g_i \gg g_c$), suddenly at $t=0$ changed g to a final value g_f , and examined the long-time development of correlations of the ferromagnetic order. (Our formalism also provided results for all $t > 0$, but we have not examined the detailed time evolution here.) The results are summarized in Fig. 5. True long-range order does not develop at any value of g_f ; however, significant order-parameter correlations do appear, and these are best formed for $g_f \approx g_c$. In a general nonintegrable system we may expect thermalization at long times, at a temperature such that the average energy equals that of the state at $t=0^+$. Such thermalization does not occur for the present integrable system, and the results have certain artifacts associated with this: the long-time correlations have an oscillatory spatial dependence for $g_f < g_c$.

In the remainder of the paper we studied the nonequilibrium dynamics of models introduced in a previous paper [5] which addressed the response of a bosonic Mott insulator to a change in a strong potential gradient [1]. These models exhibit a number of quantum critical points associated with the onset of Ising density wave and superfluid order. Our numerical studies here found a feature similar to that also obtained for the solvable Ising model: the order was best formed when the final parameter value was in the vicinity of the associated quantum critical point, as illustrated in Fig. 3. Here, and in Ref. [5], we have proposed this feature as the explanation for the resonant response observed by Greiner *et al.* [1] upon “tilting” a Mott insulator of bosons in an optical lattice.

ACKNOWLEDGMENTS

We thank A. G. Abanov, S. M. Girvin, L. Levitov, and A. Polkovnikov for useful discussions. This research was supported by U.S. NSF Grants Nos. DMR-0098226 and DMR-0342157.

APPENDIX: COMPUTATIONS FOR THE ISING CHAIN

The Jordan-Wigner transformation allows the Hamiltonian of an Ising chain in a transverse field g to be written as

$$H_I = \sum_k \epsilon_k \gamma_k^\dagger \gamma_k, \quad (\text{A1})$$

where γ_k is a fermionic annihilation operator (see Chap. 4 of Ref. [4]). These are related to the Jordan-Wigner fermions c_k by a Bogoliubov transformation, parametrized by angle θ_k , where

$$\tan \theta_k = \frac{\sin k}{g - \cos k}. \quad (\text{A2})$$

In the present case, we define the γ fermions as those that diagonalize the Hamiltonian for $t > 0$, with field g_f .

Since the Hamiltonian is throughout translationally symmetric, only fermionic states with opposite pseudomomentum k and $-k$ are mixed. We may therefore write the two-component column vector

$$\Gamma_k = \begin{pmatrix} \gamma_k \\ \gamma_{-k}^\dagger \end{pmatrix} \quad (\text{A3})$$

and similarly C_k for the Jordan-Wigner fermions C_k . The Bogoliubov transformation relating C_k and Γ_k is expressed as $C_k = R^x(\theta_k) \Gamma_k$, where

$$R^x(\alpha) = \cos \frac{\alpha}{2} + i \sigma^x \sin \frac{\alpha}{2} \quad (\text{A4})$$

and here σ^x is a 2×2 Pauli matrix. (These are used for conciseness of notation and should not be confused with the operators representing the “spins” of the Ising chain.)

For $t < 0$, the field is g_i and the system is taken to be in its ground state. We define the γ' fermions as those which diagonalize the Hamiltonian in the form (A1) with this field. [Similarly, θ'_k and Γ'_k are given by analogy with Eqs. (A2) and (A3).]

The state $|\psi\rangle$ is therefore the vacuum of γ' fermions: in matrix notation,

$$\langle \psi | \Gamma'_k \Gamma_k^\dagger | \psi \rangle = \begin{pmatrix} 1 & 0 \\ 0 & 0 \end{pmatrix} = \frac{1}{2}(\sigma^z + 1). \quad (\text{A5})$$

Applying the Bogoliubov transformation to C_k and then Γ_k gives

$$\langle \psi | \Gamma_k \Gamma_k^\dagger | \psi \rangle = R^{x\dagger}(\theta_k - \theta'_k) \frac{1}{2}(\sigma^z + 1) R^x(\theta_k - \theta'_k). \quad (\text{A6})$$

Using $R^{x\dagger}(\alpha) \sigma^z R^x(\alpha) = \sigma^z \cos \alpha - \sigma^y \sin \alpha$ with $\phi_k = \theta_k - \theta'_k$ gives

$$\langle \psi | \Gamma_k \Gamma_k^\dagger | \psi \rangle = \frac{1}{2} (1 + \sigma^x \cos \phi_k - \sigma^y \sin \phi_k), \quad (\text{A7})$$

as the set of matrix elements for the initial state.

The time evolution of the operators now proceeds (using the Heisenberg picture) according to the Hamiltonian (A1) so that $\Gamma_k(t) = U_k(t) \Gamma_k(0)$, where

$$U_k(t) = \begin{pmatrix} e^{-i\epsilon_k t} & 0 \\ 0 & e^{i\epsilon_k t} \end{pmatrix} = R^{z\uparrow}(2\epsilon_k t). \quad (\text{A8})$$

The expectation values at any time can therefore be evaluated using the algebra of SU(2) matrices.

The n -site correlator can be written as $\langle G_n \rangle = \langle B_0 A_1 B_1 \cdots B_{n-1} A_n \rangle$, where $A_i = c_i^\dagger + c_i$ and $B_i = c_i^\dagger - c_i$. Wick's theorem can then be used to write this expression in terms of the expectation values of expressions bilinear in A_i and B_i . We therefore let

$$\Omega_k(t) = \begin{pmatrix} A_k(t) \\ B_k(t) \end{pmatrix} = \sqrt{2} R^y \left(\frac{\pi}{2} \right) C_k(t), \quad (\text{A9})$$

where A_k (B_k) is the Fourier transform of A_i (B_i) so that

$$\langle \psi | \Omega_k \Omega_k^\dagger | \psi \rangle = \langle \psi | \begin{pmatrix} A_k A_{-k} & -A_k B_{-k} \\ B_k A_{-k} & -B_k B_{-k} \end{pmatrix} | \psi \rangle = 2R^y \left(\frac{\pi}{2} \right) \langle \psi | C_k C_k^\dagger | \psi \rangle R^{y\uparrow} \left(\frac{\pi}{2} \right), \quad (\text{A10})$$

$$= 1 - \sigma^x (\cos \theta_k \cos \phi_k - \sin \phi_k \sin \theta_k \cos 2\epsilon_k t) + \sigma^y (\sin \theta_k \cos \phi_k + \sin \phi_k \cos \theta_k \cos 2\epsilon_k t) + \sigma^z (\sin \phi_k \sin 2\epsilon_k t), \quad (\text{A11})$$

$$= \begin{pmatrix} 1 - \sin \phi_k \sin 2\epsilon_k t & -e^{i\theta_k} (\cos \phi_k + i \sin \phi_k \cos 2\epsilon_k t) \\ -e^{-i\theta_k} (\cos \phi_k - i \sin \phi_k \cos 2\epsilon_k t) & 1 + \sin \phi_k \sin 2\epsilon_k t \end{pmatrix}. \quad (\text{A12})$$

Transforming to real space and using the conservation of pseudomomentum gives

$$\langle A_l A_j \rangle = \frac{1}{M} \sum_k e^{ik(l-j)} (1 - \sin \phi_k \sin 2\epsilon_k t), \quad \langle B_l B_j \rangle = \frac{1}{M} \sum_k e^{ik(l-j)} (-1 - \sin \phi_k \sin 2\epsilon_k t), \quad (\text{A13})$$

$$\langle B_l A_j \rangle = \frac{1}{M} \sum_k e^{ik(l-j)} e^{-i\theta_k} (-\cos \phi_k + i \sin \phi_k \cos 2\epsilon_k t).$$

The long-time averages of these expressions are

$$\langle A_l A_j \rangle = \delta_{lj}, \quad \langle B_l B_j \rangle = -\delta_{lj}, \quad \langle B_l A_j \rangle = a_{l-j+1}, \quad (\text{A14})$$

where

$$a_r = \frac{1}{M} \sum_k e^{-ikr} \tilde{a}(k) \quad (\text{A15})$$

$$= \frac{1}{2\pi} \int_{-\pi}^{\pi} e^{-ikr} \tilde{a}(k), \quad (\text{A16})$$

in the limit where the number of sites M becomes infinite. Here, $\tilde{a}(k) = -e^{i(\theta_k + k)} \cos(\theta_k - \theta'_k)$. Wick's theorem then allows the expression for $\langle G_n \rangle$ to be written as Eq. (11).

-
- [1] M. Greiner, O. Mandel, T. Esslinger, T. W. Hänsch, and I. Bloch, *Nature (London)* **415**, 39 (2002).
 [2] C. Orzel, A. K. Tuchman, M. L. Fenselau, M. Yasuda, and M. A. Kasevich, *Science* **291**, 2386 (2001).
 [3] M. P. A. Fisher, P. B. Weichman, G. Grinstein, and D. S.

Fisher, *Phys. Rev. B* **40**, 546 (1989).

- [4] For a review, S. Sachdev, *Quantum Phase Transitions* (Cambridge University Press, Cambridge, England, 1999), Chap. 11.
 [5] S. Sachdev, K. Sengupta, and S. M. Girvin, *Phys. Rev. B* **66**, 075128 (2002).

- [6] K. Braun-Munzinger, J. A. Dunningham, and K. Burnett, e-print cond-mat/0211701.
- [7] F. Iglói and H. Rieger, Phys. Rev. Lett. **85**, 3233 (2000).
- [8] P. Fendley, K. Sengupta, and S. Sachdev, Phys. Rev. B **69**, 075106 (2004).
- [9] M. E. Fisher and R. E. Hartwig, Adv. Chem. Phys. **15**, 333 (1968); E. L. Basor and C. A. Tracy, J. Phys. A **177**, 167 (1991); T. Ehrhardt, J. Oper. Theory **124**, 217 (2001).
- [10] E. Altman and A. Auerbach, Phys. Rev. Lett. **89**, 250404 (2002).
- [11] A. Polkovnikov, S. Sachdev, and S. M. Girvin, Phys. Rev. A **66**, 053607 (2002).
- [12] L. S. Levitov (private communication). Note that our Hamiltonian (26) has a certain resemblance to the BCS theory, but we are considering bosons subject to the hard-core constraints (28), rather than fermions.